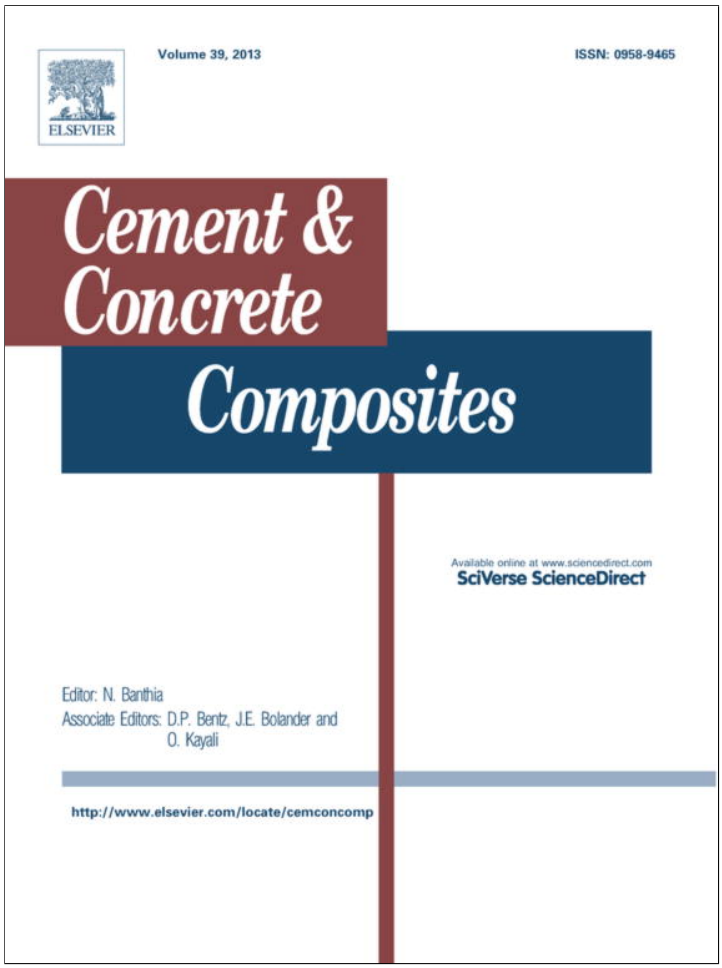

Cement & Concrete Composites 39 (2013) 23–32

Contents lists available at SciVerse ScienceDirect

Cement & Concrete Composites

journal homepage: www.elsevier.com/locate/cemconcomp

A comparison study of Portland cement hydration kinetics as measured by chemical shrinkage and isothermal calorimetry

Xueyu Pang [a,*], Dale P. Bentz [b], Christian Meyer [c], Gary P. Funkhouser [a], Robert Darbe [a]

[a] Halliburton, 3000 N Sam Houston Pkwy E, Houston, TX 77032, USA
[b] Engineering Laboratory, National Institute of Standards and Technology, USA
[c] Department of Civil Engineering and Engineering Mechanics, Columbia University, USA

ARTICLE INFO

Article history:
Received 29 November 2012
Received in revised form 7 February 2013
Accepted 20 March 2013
Available online 28 March 2013

Keywords:
Cement hydration
Kinetics
Chemical shrinkage
Heat of hydration
Isothermal calorimetry
Oilwell cement

ABSTRACT

Two different methods of evaluating cement hydration kinetics, namely chemical shrinkage and isothermal calorimetry tests, are used to investigate the early stage hydration of different classes of oilwell cement at various temperatures. For a given cement paste, the hydration kinetics curves measured by the two methods are proportional to each other at the same curing temperature. The ratio of heat of hydration to chemical shrinkage for different cements used in this study ranges from 7500 J/mL to 8000 J/mL at 25 °C and increases almost linearly with increasing curing temperature at a rate that varies only slightly with cement composition (approximately 58 J/mL per °C). A previously proposed scale factor model for simulating the effect of curing temperature and pressure on cement hydration kinetics is further validated in this study for its temperature aspect. The model is shown to be particularly helpful in correcting for slight temperature errors in the experiments.

1. Introduction

The hydration of Portland cement is a complex process. Despite decades of research, many detailed features are still not clearly understood today, primarily because of the complicating influences of different clinker phases, impurities, and their interactions. Nevertheless, the general hydration kinetics of cement is often represented by the rate of change of the overall degree of hydration α, which is defined as the total weight fraction of cement reacted. As a composite material consisting mainly of four compounds, or clinker phases (C_3S, C_2S, C_3A and C_4AF[1]), the overall degree of hydration of cement is typically written as [1]:

$$\alpha(t) = p_{C_3S}\alpha_{C_3S}(t) + p_{C_2S}\alpha_{C_2S}(t) + p_{C_3A}\alpha_{C_3A}(t) + p_{C_4AF}\alpha_{C_4AF}(t) \quad (1)$$

where p_i is the original weight fraction of *Phase i* in the anhydrous cement and $\alpha_i(t)$ is the degree of hydration of *Phase i* at time *t*. Direct determination of $\alpha_i(t)$ can be made by quantitative X-ray diffraction analysis (QXDA) [1,2], though it is difficult to obtain accurate results. Some properties of a hydrating cement paste, such as the non-evaporable water content, the cumulative heat evolution and the total chemical shrinkage have been shown to have approximately linear relationships with the overall degree of hydration [1,3–5]. As a matter of fact, α is more easily and commonly determined indirectly by tracking the time dependence of one or more of these properties. For the purposes of this paper, the semi-continuous measure of the progress of the degree of hydration with time ($\alpha(t)$) and its derivative ($d\alpha(t)/dt$) are both referred to as the hydration kinetics curves.

Among the different methods of approximating cement hydration progress, heat of hydration tests used to be the only one that provided continuous data suitable for evaluating hydration mechanisms. Automated chemical shrinkage test methods have been developed in recent years [6–9] and are now also frequently used to study cement hydration mechanisms [9–12]. Therefore, it is important to investigate the differences and similarities between these two different methods, which may also help us gain further insights about the cement hydration process. In this study, both the traditional isothermal calorimetry and one of the newly developed chemical shrinkage test methods were employed to measure the hydration kinetics of cement at similar curing conditions and a detailed comparison of the two sets of test results was performed.

The experimental test methods and detailed test plan of this study are described Section 2. The theoretical analysis regarding the correlation between heat of hydration and chemical shrinkage is presented in Section 3. Because temperature control of the chemical shrinkage tests performed in this study was not very accurate, a method of correcting the temperature differences between isothermal calorimetry tests and chemical shrinkage tests

* Corresponding author.
E-mail address: Xueyu.Pang@halliburton.com (X. Pang).

[1] Cement chemistry notation: C = CaO, S = SiO_2, H = H_2O, A = Al_2O_3, F = Fe_2O_3.

0958-9465/$ - see front matter © 2013 Elsevier Ltd. All rights reserved.
http://dx.doi.org/10.1016/j.cemconcomp.2013.03.007

is also proposed in Section 3 based on a scale factor model developed earlier. The scale factor model was developed to simulate the effect of curing temperature and pressure on cement hydration kinetics and has been preliminarily validated using chemical shrinkage test data [12]. When the hydration kinetics curve of a reference curing temperature is known for a given cement paste, the scale factor model can be used to estimate the hydration kinetics curve for a given temperature or the temperature of a given hydration kinetics curve. In Section 4.1, the model is further validated with isothermal calorimetry test data from this study. Since the rate of hydration is measured directly in these tests, the accuracy and limitations of the scale factor model can be observed and discussed in greater detail. In Section 4.2, it is shown that the hydration kinetics measured by chemical shrinkage can be correlated excellently with those measured by isothermal calorimetry by applying the proposed model in this study.

2. Materials and methods

2.1. Materials

Oilwell cements are based upon Portland cement, but manufactured to a higher level of consistency from one production batch to another. There are no substantial differences between oilwell cements and ordinary Portland cements, except for the fact that some Class H (API Specification 10A [13]) cement may have near zero C_3A content. API Classes A, B, and C cements are similar to ASTM Types I, II, and III cements, respectively. The hydration kinetics of four different classes of oilwell cements, namely Classes A, C, G, and H, were investigated at different curing temperatures in this study. All slurries (cement pastes) were prepared with de-aerated water and cement only, with no additives. As will be shown in Section 2.2, standard water-to-cement (w/c) mass ratios for each class of cement were used, as defined in API Specification 10A [13]. The main compound compositions of the different types of cements derived from the oxide analysis test results using the Bogue calculation method [14] are presented in Table 1. As shown in the table, two different types of Class H cements were used: a premium Class H (H-P) and a standard Class H. Some minor composition variations were observed between different batches of standard Class H cement (H-I and H-II) produced from the same plant.

The particle size distributions of the cements were measured by the laser scattering technique with dry dispersion methods (at least 10 measurements were performed on each type of cement). The average test results are presented in Fig. 1 (Class H-I cement was not measured as it should be similar to Class H-II cement). The median particle sizes for Classes A, C, G, H-P, and H-II cements were 38 μm, 15 μm, 34 μm, 30 μm, and 23 μm, respectively, while their specific surface areas calculated from the PSD data (assuming spherical particles and a cement density of 3150 kg/m^3) were 356 m^2/kg, 565 m^2/kg, 327 m^2/kg, 394 m^2/kg, and 323 m^2/kg, respectively. Apparently, the median particle size does not necessarily correlates with the specific surface area since the latter is primarily dominated by the relative proportion of the fine particles. The particle size distribution curves for the Class A, G, and H-P cements are very similar, suggesting that similar grinding procedures may have been adopted in manufacturing these cements. Class C cement is ground much finer than the other classes to achieve a higher specific surface area and enhance early-age reactivity.

Table 1
Estimated main compound compositions (by mass percentage) of the different cements.

Cement	C_3S	C_2S	C_3A	C_4AF	C_2F	$CaSO_4$	Free lime
A	61.7	12.0	8.4	9.4	0	4.7	1.4
C	72.2	5.2	2.2	11.8	0	4.7	0.2
G	62.6	15.9	4.8	10.9	0	3.8	0.2
H-P	47.9	27.5	0	16.2	2.0	4.2	0.3
H-I	66.5	11.7	0.3	13.4	0	4.5	0.3
H-II	70.3	8.5	0	12.8	0.0	4.8	0.3

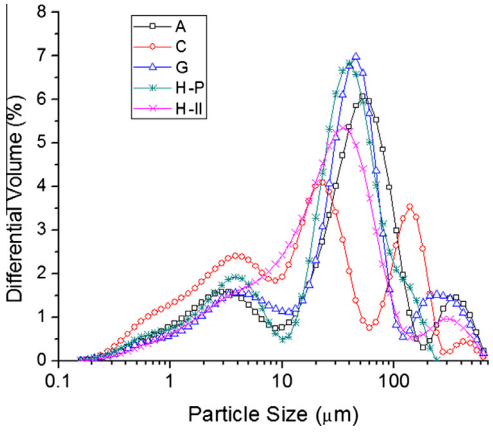

Fig. 1. Particle size distributions of different classes of cements.

2.2. Chemical shrinkage test

The total absolute volume of cement hydration product is smaller than the combined initial volume of the anhydrous cement and water. This reduction in volume during hydration is known as chemical shrinkage. Despite the apparently simple principle of chemical shrinkage measurement, there are experimental difficulties that can yield spurious results. For example, the traditional chemical shrinkage test (ASTM C1608 [15]) involves adding a significant amount of water on top of a thin specimen (<10 mm) to keep it saturated. A recent study showed that the quantity and the composition of the surface water have a significant impact on test results [16]. Increasing the amount of surface water was found to increase the chemical shrinkage rate before the end of the induction period and to reduce the peak chemical shrinkage rate during later periods. The initial increase is probably due to the accelerated dissolution as a result of more Ca^{2+} leaching out of the paste sample (and into the surface water solution), while the reduced peak rate might be related to a dilution effect. Massive precipitates of portlandite were observed on the surface of specimens of alite (the main composition of Portland cement) used for chemical shrinkage measurement [17]. Additionally, when the same measuring device was used, increasing sample thickness was consistently found to cause a reduction in chemical shrinkage at later ages (>15 h) [6,16,17]. This thickness effect may be explained by two hypotheses: (1) the reduction in the permeability of the sample might prevent surface water from filling all the pores in the thicker samples (depercolation); (2) a larger fraction of the thinner sample is diluted by the surface water, resulting in a faster hydration rate at later ages. Costoya [17] found that using a small diameter device with less surface water (cylindrical flask) systematically gave a higher chemical shrinkage of a given mass of alite paste than when the same mass of paste was used in a large diameter device with more surface water (Erlenmeyer flask), even though the former generated a much thicker sample. The author also found that chemical shrinkage measured with the former device was the same as that measured with a set ground paste sample for a period exceeding 250 h. Therefore, for cement pastes with relatively high w/c ratios, surface water probably has a much stronger effect on the test result than the thickness of the sample and the latter is probably not a limiting factor.

Table 2
Chemical shrinkage tests (test series I, test duration = 72 h).

Curing temperature (°C)		Ambient[a]	40.6[b]	60[b]
Cement	*w/c*	–	–	–
A	0.46	CS-A-1	CS-A-2	CS-A-3
C	0.56	CS-C-1	CS-C-2	CS-C-3
G	0.44	CS-G-1	CS-G-2	CS-G-3
H-P	0.38	CS-HP-1	CS-HP-2	CS-HP-3
H-I	0.38	CS-H-1	CS-H-2	

[a] Lab temperature (~24 ± 2.8 °C).
[b] Estimated specimen temperature (will be corrected later based on test results).

In this study, chemical shrinkage was measured by a recently developed test apparatus [18] originally designed to obtain in situ tensile strength of oilwell cements at different curing pressures. The apparatus allows automatic collection of chemical shrinkage data from samples cured at different temperatures and pressures. In addition, by using a large volume of cement paste (four 51 mm by 170 mm cylinders), the effect of surface water on test results is expected to be minimal. When a hydrostatic curing pressure of 0.69 MPa was applied, tests performed using hollow cylinders (whose entire annular surfaces were covered by filter paper for water saturation) with a wall thickness of approximately 10 mm were found to generate the same results as solid cylinders [18], suggesting sample thickness is not a limiting factor of test results for this type of test under the conditions being employed. The test design of the chemical shrinkage test series is shown in Table 2. The main shortcoming of this new test apparatus is the lack of precise temperature control. Fortunately, as will be discussed later, any slight temperature errors can be accounted for with a scale factor when the test results are correlated with those of the isothermal calorimetry tests. Test data oscillation also seems to be dramatically increased when heating devices are employed for high temperature tests, and such oscillations make it difficult to calculate reliable derivative curves directly from cumulative experimental data. Uncertainties in test results caused by factors other than temperature fluctuations are estimated to be less than 3% at the end of 3 d. More detailed uncertainty analysis of this experimental technique is given in [18].

2.3. Isothermal calorimetry test

Compared to chemical shrinkage, isothermal calorimetry is a more established test method of measuring overall cement hydration progress. In the second test series, hydration of the different types of cements is tracked with an isothermal calorimeter according to standard test procedures [19]. Tests were conducted at atmospheric pressure and three different curing temperatures. Table 3 shows the test design for this test series. The temperatures of isothermal calorimetry tests can be controlled more precisely due to the small sample size (4–5 g). For this technique, the average absolute difference between replicate specimens of cement paste is 2.4×10^{-5} W/g (cement), with a maximum absolute difference of 0.00011 W/g (cement), for measurements conducted between 1 h and 7 d after mixing [20]. It should be mentioned that the samples used in the isothermal calorimetry tests were cured under sealed condition, which is different from the saturated curing condition for the chemical shrinkage tests. Although it is difficult to accurately evaluate the effect of saturation condition on the isothermal calorimetry test results due to various experimental difficulties, a previous study [5] suggests that saturation has a negligible effect on tests with relatively high *w/c* ratios (the small differences in tests results were probably caused by the surface water effect discussed in Section 2.2).

Table 3
Isothermal calorimetry tests (test series II, test duration = 168 h).

Curing temperature (°C)		25	40	60
Cement	*w/c*	–	–	–
A	0.46	IC-A-1	IC-A-2	IC-A-3
C	0.56	IC-C-1	IC-C-2	IC-C-3
G	0.44	IC-G-1	IC-G-2	IC-G-3
H-P	0.38	IC-HP-1	IC-HP-2	IC-HP-3
H-I	0.38	IC-H-1	IC-H-2	IC-H-3

3. Theoretical background and analysis

3.1. Indirect methods of measuring cement hydration

When the indirect methods are employed to measure cement hydration progress, the relationships between experimental results and the overall degree of hydration can be expressed as [9,21–25]:

$$\alpha(t) = \frac{w_n(t)}{w_n^0} = \frac{H(t)}{H^0} = \frac{CS(t)}{CS^0} \tag{2}$$

where $w_n(t)$ and w_n^0 are the non-evaporable water content at time t and at complete hydration, respectively (typically in g/g cement); $H(t)$ and H^0 are the cumulative heat evolution at time t and at complete hydration, respectively (typically in J/g cement); and $CS(t)$ and CS^0 are the total chemical shrinkage at time t and at complete hydration, respectively (typically in mL/g cement). w_n^0 depends on the molar masses of the hydration products, while H^0 depends on the enthalpy changes of the chemical reactions, both of which are expected to remain constant as long as the chemical formulae of the hydration products do not change. However, CS^0 depends on the molar volumes of water and the hydration products and hence varies with both temperature and pressure. According to Eq. (2), since w_n^0 and H^0 remain invariant (at least within the temperature and pressure range used in this study), the dependency of CS^0 on temperature and pressure can be approximately evaluated by studying the correlations between $w_n(t)$, $H(t)$, and $CS(t)$ at various curing conditions. Studies have shown that the ratio of $CS(t)$ to $w_n(t)$, evaluated at discrete data points, decreases with increasing temperature [6,10], suggesting that CS^0 decreases with increasing temperature. The focus of this study is the correlation between $CS(t)$ and $H(t)$, both of which have been measured continuously.

It should be pointed out that the indirect methods only give a gross approximation to the hydration rate of cement because hydration of the different phases also progresses at different rates. If we ignore the interactions between different clinker phases and the phase changes of different hydration products during hydration, then the total heat of hydration and chemical shrinkage may be correlated with the degree of hydration of each individual clinker phase as follows,

$$H(t) = a_{C_3S}p_{C_3S}\alpha_{C_3S}(t) + a_{C_2S}p_{C_2S}\alpha_{C_2S}(t) + a_{C_3A}p_{C_3A}\alpha_{C_3A}(t) + a_{C_4AF}p_{C_4AF}\alpha_{C_4AF}(t) \tag{3}$$

$$CS(t) = b_{C_3S}p_{C_3S}\alpha_{C_3S}(t) + b_{C_2S}p_{C_2S}\alpha_{C_2S}(t) + b_{C_3A}p_{C_3A}\alpha_{C_3A}(t) + b_{C_4AF}p_{C_4AF}\alpha_{C_4AF}(t) \tag{4}$$

where a_i, and b_i are the cumulative heat evolution and the total chemical shrinkage, respectively, associated with the complete hydration of 1 g of clinker *phase i*. Eqs. (3) and (4) can be used to estimate the parameters associated with the complete hydration condition in Eq. (2), using the sums

$$H^0 = \sum a_i p_i, CS^0 = \sum b_i p_i \tag{5}$$

Table 4
Coefficients for estimating the parameters at the complete hydration condition.

Phase	C_3S	C_2S	C_3A	C_4AF	Reference
a_i (J/g)[a]	510	247	1356	427	[28]
b_i (mL/g at 25 °C)	0.0596	0.0503	0.13	0.0469	[9]
a_i/b_i	8557	4911	10,431	9104	

[a] Obtained by multi-linear regression analysis from experimental data of 21 different cements, slightly different from theoretical values calculated from standard enthalpy of formation [28,29], which depend on the chemical formulae of hydration products.

Eq. (2) is only exact either when all the different clinker phases hydrate at the same rate or when the coefficients (i.e. a_i's and b_i's) associated with different phases are the same, neither of which is true [26,27]. Nevertheless, Eq. (2) is still widely used as acceptable approximations [9,21–25]. In addition, if the ratios of the coefficients associated with different clinker phases are constant, that is,

$$\frac{a_{C_3S}}{b_{C_3S}} = \frac{a_{C_2S}}{b_{C_2S}} = \frac{a_{C_3A}}{b_{C_3A}} = \frac{a_{C_4AF}}{b_{C_4AF}} \tag{6}$$

then the following part of Eq. (2) will still be exact,

$$\frac{H(t)}{H^0} = \frac{CS(t)}{CS^0} \tag{7}$$

Accurate determination of the coefficients (i.e. a_i, and b_i) for each individual phase is challenging because complete hydration of all clinker phases is difficult to achieve and estimation of the phase compositions (i.e., p_i) are usually not accurate. Recent estimates (Table 4) suggest that Eq. (6) is approximately true for three out of four main clinker phases (C_3S, C_3A, C_4AF). Therefore, Eq. (7) should provide a reasonable approximation, especially for early age hydration, which is typically dominated by C_3S and C_3A.

3.2. A scale factor model for the effect of curing conditions on cement hydration

When the time dependence of the degree of hydration of cement is represented by an unknown function, the effect of curing temperature and pressure can be modeled by incorporating a scale factor C into that function [12]. For example, if hydration at the reference temperature T_r and pressure P_r is represented by the following functions,

$$\text{Integral curve} : \alpha = \alpha_{T_r,P_r}(t), \quad \text{Derivative curve} : d\alpha/dt = \alpha'_{T_r,P_r}(t) \tag{8}$$

then the transformed functions at temperature T and pressure P are

$$\begin{aligned} \text{Integral curve} &: \alpha = \alpha_{T,P}(t) = \alpha_{T_r,P_r}(Ct), \\ \text{Derivative curve} &: d\alpha/dt = \alpha'_{T,P}(t) = C \cdot \alpha'_{T_r,P_r}(Ct) \end{aligned} \tag{9}$$

The scale factor is similar to the coefficient used to compute the equivalent age of a specified curing condition when applying the maturity method to estimate concrete strength (ASTM C1074 [30]). It is important to note that both the scale factor model and the equivalent age method assume the hydration mechanism do not change over the ranges of temperature and pressure studied. The dependence of the scale factor on curing temperature can be modeled by the following equation [12],

$$C_{T_r-T,P_r-P} = \exp\left(\frac{E_a}{R}\left(\frac{1}{T_r}-\frac{1}{T}\right) + \frac{\Delta V^{\ddagger}}{R}\left(\frac{P_r}{T}-\frac{P}{T}\right)\right) \tag{10}$$

where E_a is the apparent activation energy (J/mol); $\Delta V^{\ddagger}$ is the apparent activation volume (m^3/mol); R is the universal gas constant (8.314 J/(mol K)); T and P are the temperature (K) and pressure (Pa) of an arbitrary curing condition, while T_r and P_r are the temperature (K) and pressure (Pa) of the reference curing condition; C is the scale factor associated with temperature change from T_r to T and pressure change from P_r to P.

One of the most important advantages of the scale factor model is that it is very straightforward and easy to use. The physical meaning of the model is that the hydration rate at any curing condition is increased or decreased by a factor of C compared with that at the reference curing condition at the same degree of hydration. Probably due to the different mechanism of hydration during the very early period (before the end of the induction period), it is sometimes necessary to offset the predicted hydration kinetics curve using the scale factor model to generate a better agreement with the experimental curve, especially when their curing temperatures are different. The offset is not necessary for tests performed at different curing pressures in the range from 0.7 MPa to 51.7 MPa [12]. Therefore, a more accurate representation of the relationship between the hydration kinetics curves at temperatures T and T_r (for the same curing pressure) is,

$$\begin{aligned} \text{Integral Curves} &: \alpha_T(t) = \alpha_{T_r}(C_{T_r-T} \cdot (t-t_0)) \\ \text{Derivative Curves} &: \alpha'_T(t) = C_{T_r-T} \cdot \alpha'_{T_r}(C_{T_r-T} \cdot (t-t_0)) \end{aligned} \tag{11}$$

where α_T and α_{T_r} are the functions representing the time dependence of the degree of hydration at temperatures T and T_r, respectively; t_0 is the offset time, which appears to increase with increasing differences between T_r and T; C_{T_r-T} is the scale factor related to the temperature differences, which is the same as defined in Eq. (10) at constant pressure,

$$C_{T_r-T} = \exp\left(\frac{E_a}{R}\left(\frac{1}{T_r}-\frac{1}{T}\right)\right) \tag{12}$$

3.3. Correlation between heat of hydration and chemical shrinkage

If we consider an isothermal calorimetry test performed at temperature T_{IC} and a chemical shrinkage test performed at temperature T_{CS}, the degree of hydration measured by the former can be expressed as,

$$\alpha_{T_{IC}}(t) = \frac{H_{T_{IC}}(t)}{H^0} \tag{13}$$

while that measured by the latter can be expressed as,

$$\alpha_{T_{CS}}(t) = \frac{CS_{T_{CS}}(t)}{CS^0(T_{CS})} \tag{14}$$

Note that, as already discussed, CS^0 is a function of temperature. Employing the scale factor model, one can obtain,

$$\alpha_{T_{IC}}(t) = \alpha_{T_{CS}}(C_{T_{CS}-T_{IC}}(t-t_0)) \tag{15}$$

where the scale factor is related to the temperature difference between the two types of tests by the following equation,

$$C_{T_{CS}-T_{IC}} = \exp\left(\frac{E_a}{R}\left(\frac{1}{T_{CS}}-\frac{1}{T_{IC}}\right)\right) \tag{16}$$

By combining Eqs. (13)–(15), the cumulative heat evolution $H(t)$ can be related to the total chemical shrinkage $CS(t)$ by the following equation,

$$H_{T_{IC}}(t) = \frac{H^0}{CS^0(T_{CS})} CS_{T_{CS}}(C_{T_{CS}-T_{IC}}(t-t_0)) \tag{17}$$

4. Test results and discussion

4.1. Validation of the scale factor model

One of the most important assumptions of the scale factor model is that the normalized rate of hydration vs. degree of hydration

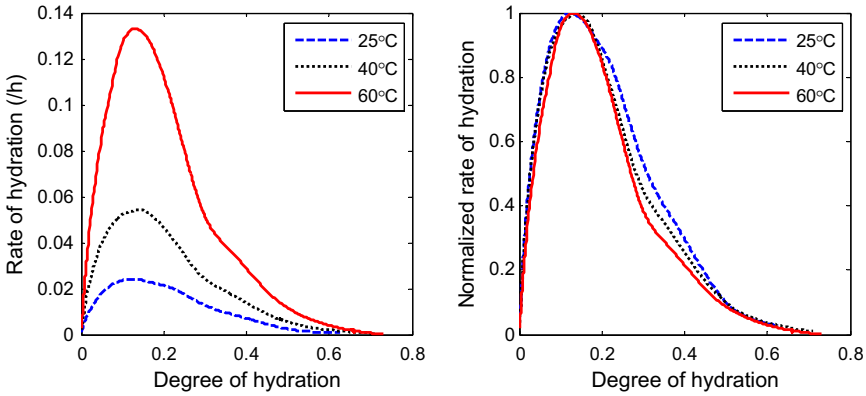

Fig. 2. Effect of curing temperature on hydration rate as a function of degree of hydration (Class H-I cement, $w/c = 0.38$).

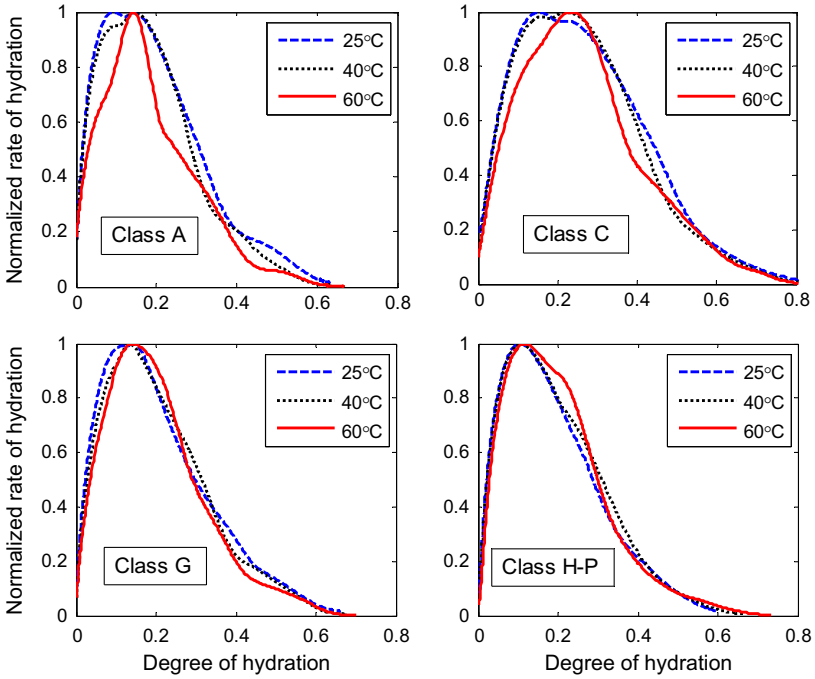

Fig. 3. Normalized rate of hydration vs. degree of hydration of different cements.

curve of a given cement paste is invariant with curing condition (for isothermal and isobaric tests). The assumption has been verified for different types of cement in the pressure range from 0.7 to 51.7 MPa using chemical shrinkage test data [12]. Oscillations of chemical shrinkage test results at high temperatures made it difficult to derive the rate of hydration accurately. Therefore, further validation of this assumption is desirable for different curing temperatures with the heat evolution data. Based on the values listed in Table 4 and assuming C_2F generates the same amount of heat as C_4AF on the same mass basis, the cumulative heat generated at complete hydration (H^0) was estimated to be 497.7 J/g (cement), 461.1 J/g, 470.1 J/g, 429.2 J/g, and 385.9 J/g, for Classes A, C, G, H-I, and H-P cements, respectively. The hydration progress of these different types of cement can be obtained by normalizing the heat evolution data by their respective H^0 values.

It should be pointed out that the scale factor model was developed for a single reaction process assuming that the curing condition only changes the rate of the reaction, but not its nature. In reality, Portland cement hydration is a much more complex process with all the different clinker phases having different reaction rates as well as different sensitivities to curing temperature changes (i.e., activation energies). The composition of the hydration products may also change if curing temperature changes significantly. Therefore, the model can be applied only approximately to analyze Portland cement hydration. Fig. 2 shows the rate of hydration vs. degree of hydration derived from the heat evolution data of Class H-I cement before and after normalization. While the normalized data at different curing temperatures coincide relatively well during early and late periods, slight deviations are observed during the middle period, (i.e., for degrees of hydration approximately ranging from 0.2 to 0.5). Fig. 3 shows the normalized rate of hydration vs. degree of hydration of the four other types of cement obtained at different curing temperatures. Similar convergence behaviors were observed except for the Class A and Class C cements at 60 °C, both of which diverge significantly from their behavior at 25 °C and 40 °C. For all the different types of cement, the divergences of the normalized kinetics curves becomes more significant as the temperature difference increases, due to the different temperature sensitivities of different phases. The normalized hydration data at 25 °C and 40 °C appear to show better

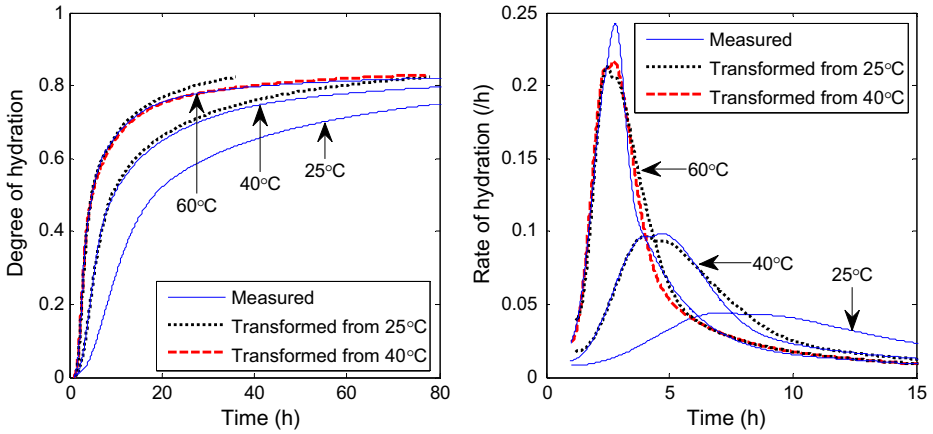

Fig. 4. Measured and predicted hydration kinetics at different curing temperatures by coordinate transformations (Class C cement, $w/c = 0.56$).

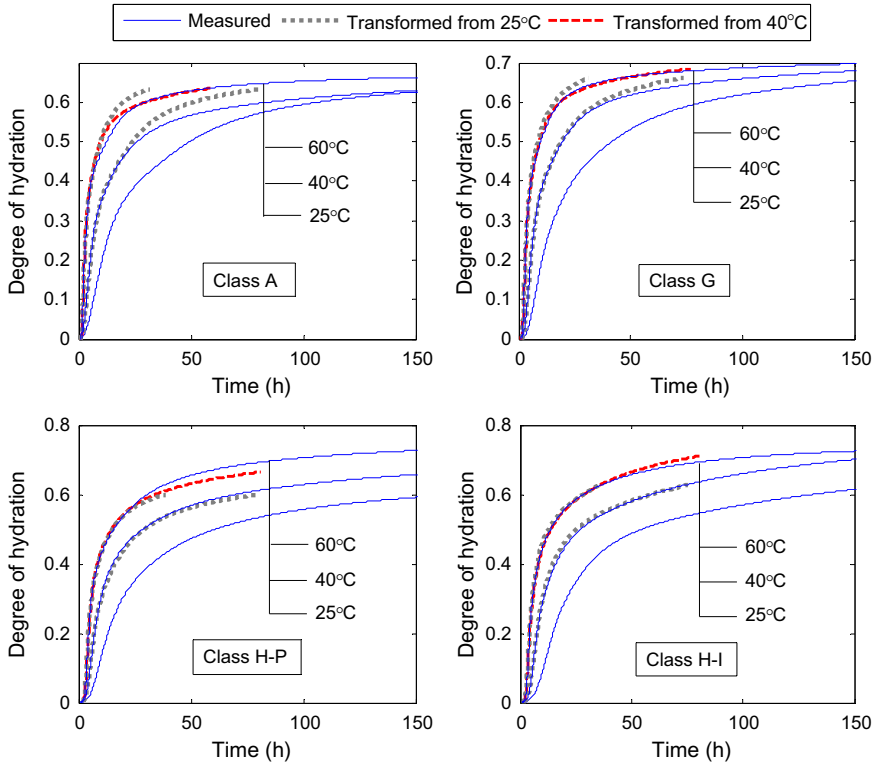

Fig. 5. Measured and predicted hydration kinetics of different cements at different curing temperatures by coordinate transformations.

compliance with the model, indicating that the scale factor model is more accurate for relatively small temperature changes.

According to Eq. (11), the scale factor relating the hydration rates at two different curing temperatures can be estimated by applying basic coordinate transformation rules to transform the hydration kinetics curve at T_r to achieve the best agreement with that at T (the method is referred to as the best fit method). Fig. 4 shows the results of transforming the experimental hydration data obtained at 25 °C and 40 °C to fit/predict those at higher curing temperatures for Class C cement. Although it seems impossible to achieve perfect agreement for the entire curing period, the predictions are in good agreements with the actual experimental results during the period up to the first peak, which is mainly associated with C_3S hydration. The second peak probably includes the contribution from C_3A hydration, which reportedly has a higher activation energy than the overall value for Portland cement [31,32]. Therefore, the transformed hydration data from lower temperatures typically underestimate the second peak (Fig. 4). Applying a different scale factor for each individual phase in Portland cement would perhaps generate a better fit. Unfortunately, it is not yet possible to accurately and reliably measure the hydration progress of the different phases separately.

Fig. 5 shows the measured and predicted hydration kinetics curves for the other types of cement used in this study. The predictions are most accurate for the Class H-I cement, which has almost no C_3A, and least accurate for the Class A cement, which has the highest C_3A content. This further confirms the hypothesis that a higher C_3A activation energy can skew the model results. It is also interesting to note that the transformed data from lower temperatures typically overestimate slightly the degree of hydration at

Table 5
Activation energies obtained from different analysis methods.

Cement	$T_r - T$ (°C)	Best fit method			Peak hydration rate method		E_a (kJ/mol) (from [12])
		t_0 (h)	C_{T_r-T}	E_a (kJ/mol)	C_{T_r-T}	E_a (kJ/mol)	
A	25–40	0.4	2.1	38.4	2.28	42.7	52.6
	25–60	0.8	5.5	40.2	7.04	46.1	
	40–60	0.8	2.9	46.2	3.09	48.9	
C	25–40	0.75	2.18	40.3	2.23	41.5	48.8
	25–60	1	4.8	37.0	5.48	40.1	
	40–60	0.6	2.2	34.2	2.46	39.0	
G	25–40	0.9	2.3	43.1	2.37	44.7	50
	25–60	1	5.5	40.2	5.76	41.3	
	40–60	0.5	2.2	34.2	2.43	38.5	
H-P	25–40	1	2.15	39.6	2.12	38.9	42.5
	25–60	1.5	4.5	35.5	4.53	35.6	
	40–60	1.1	2.1	32.2	2.14	33.0	
H-I	25–40	1	2.26	42.2	2.26	42.2	44.3
	25–60	1.2	4.8	37.0	5.54	40.4	
	40–60	0.7	2.1	32.2	2.45	38.9	

later ages, with the exception of Class H-P cement, for which the opposite is true. Table 5 lists the offset time and scale factor, as well as the apparent activation energy (calculated from the scale factor using Eq. (12)) associated with each temperature change. The constants are obtained by trial and error to provide the best agreements as shown in Figs. 4 and 5. For comparison purposes, Table 5 also lists the scale factors and apparent activation energies calculated with the peak hydration rate method as proposed in a previous study [12]. The constants obtained by the two different methods generally agree well with each other for relatively small temperature changes (from 25 °C to 40 °C and from 40 °C to 60 °C) but may differ quite noticeably for the larger temperature change (from 25 °C to 60 °C). The apparent activation energies obtained in different temperature ranges appear to decrease with increasing temperature except for Class A cement, for which the opposite is true. The apparent activation energies obtained in this study are also found to be much lower than those calculated from chemical shrinkage test data [12]. The latter are probably less accurate due to the inadequate temperature control of the tests and errors associated with estimating CS^0 at different temperatures (H^0 is assumed to be independent of temperature).

4.2. Correlations between chemical shrinkage and heat of hydration of cement

Just as the hydration kinetics curve at a reference temperature can be transformed to fit the curves obtained at other temperatures, the chemical shrinkage curve can be transformed to fit the heat evolution curve (and vice versa) according to their correlations developed in Section 3.3. Following Eq. (17), the correlation factor $H^0/CS^0(T_{CS})$, the scale factor $C_{T_{CS}-T_{IC}}$, and the offset time t_0, can all be estimated by transforming the chemical shrinkage curve to achieve the best agreement with the heat evolution curve. Since the scale factor model is more accurate for smaller temperature changes, the temperature of the chemical shrinkage test should be close to that of the isothermal calorimetry test to obtain more reliable estimates. Fig. 6 shows the heat evolution curves of the Class H-P cement measured at 25 °C and the transformed chemical shrinkage curves (measured at lab temperature) that exhibit the best fit. The two curves agree excellently with each other except during very early stages (before the acceleration period), where the hydration rate measured by chemical shrinkage seems to be higher than that measured by heat evolution.

Fig. 7 shows the heat evolution rate curves of the other types of cement measured at 25 °C and their corresponding best-fit

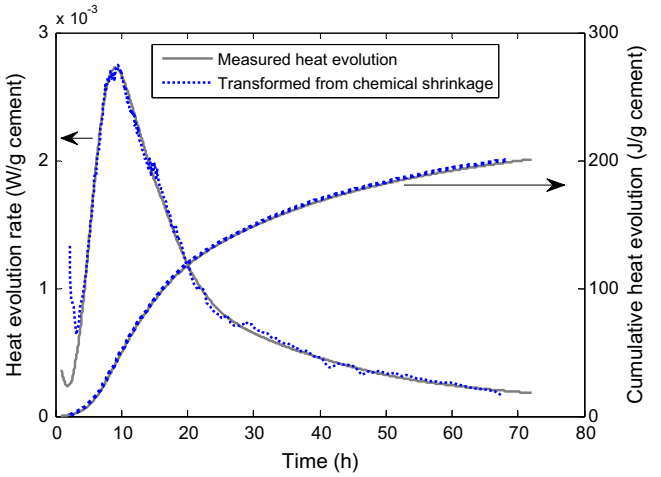

Fig. 6. Heat evolution curves vs. transformed chemical shrinkage curves (Class H-P cement, w/c = 0.38, 25 °C).

transformed chemical shrinkage curves. Similar to the Class H-P cement, excellent agreement is obtained between the heat evolution curve and the transformed chemical shrinkage curve for the Class H-I cement. However, for cements that contain significant C_3A, the agreements between the two types of curves are somewhat poorer, especially around the main hydration peaks. The hydration of C_3A first produces ettringite during the hydration peak, which then further reacts with excess C_3A and transforms to calcium monosulfoaluminate at later ages [26,28]. The test results show that the second peak rate (probably caused by C_3A hydration) measured by chemical shrinkage is always higher than that measured by heat evolution and that the rate measured by the former also decreases faster during the deceleration stage. Therefore, the ratio of chemical shrinkage to heat evolution associated with C_3A hydration is higher than that associated with C_3S hydration during the initial reaction (to form ettringite) and probably the reverse is true during the later reaction (to form monosulfoaluminate). It should be noted that the ratio of a_3 to b_3 associated with C_3A hydration as shown in Table 4 represents the long-term results of some average cements and is not strictly applicable here.

The integral curves of heat evolution of different cements cured at different temperatures are compared with the transformed chemical shrinkage curves (measured at similar temperatures) in Fig. 8. In general, excellent agreements can be obtained between

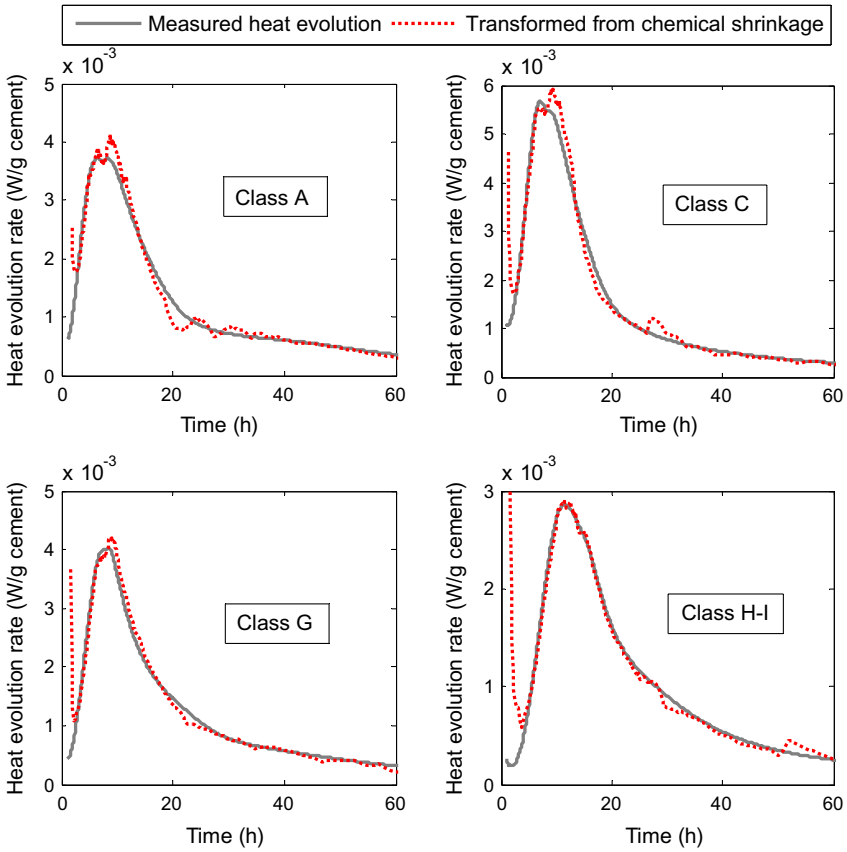

Fig. 7. Heat evolution vs. transformed chemical shrinkage for the different types of cement (derivative curves).

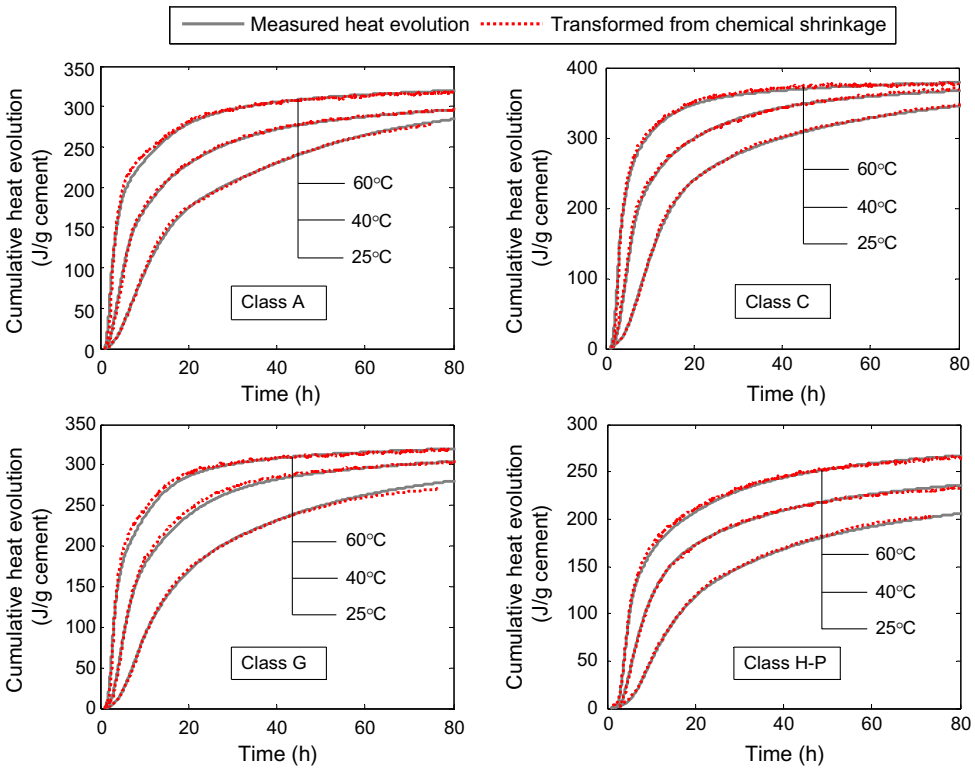

Fig. 8. Heat evolution curves vs. transformed chemical shrinkage curves for different types of cement at different curing temperatures (integral curves).

the integral hydration kinetics curves obtained from the two different methods. The constants used to transform the chemical shrinkage curves to fit the heat evolution curves, including the correlation factor, the scale factor, and the offset time, are listed

Table 6
Best-fit constants for correlating chemical shrinkage and heat evolution test results and the respective temperatures of different tests (refer to Eq. (17)).

Test no.		t_0 (h)	$C_{T_{CS}-T_{IC}}$	H^0/CS^0 (T_{CS}) (J/mL)	T_{IC} (°C)	T_{CS} (°C)
CS-A-1	IC-A-1	1	1.09	7600	25	23.4
CS-C-1	IC-C-1	0.4	0.85	7800	25	28.3
CS-G-1	IC-G-1	0.7	0.95	7700	25	25.9
CS-HP-1	IC-HP-1	1.2	1.07	7500	25	23.6
CS-H-1	IC-H-1	1	1.11	8000	25	22.9
CS-A-2	IC-A-2	0	0.84	8400	40	43.6
CS-C-2	IC-C-2	0	0.9	8350	40	42.3
CS-G-2	IC-G-2	0	0.86	8850	40	43.1
CS-HP-2	IC-HP-2	0.6	0.9	8700	40	42.4
CS-H-2	IC-H-2	0	1	8850	40	40.0
CS-A-3	IC-A-3	0	0.9	9750	60	62.4
CS-C-3	IC-C-3	0	0.9	10,100	60	62.7
CS-G-3	IC-G-3	0	0.91	9750	60	62.2
CS-HP-3	IC-HP-3	0	0.85	10,200	60	64.3

in Table 6. The cause of the offset time (primarily observed for ambient temperature tests) is not yet clear. It may be associated with variations of the duration of the induction periods, which tend to be affected by many different factors that are difficult to control. Following Eq. (16), the temperature of the chemical shrinkage test (T_{CS}) can be estimated from the more-precisely-measured temperature of the isothermal calorimetry test (T_{IC}) by using the scale factor and the previously obtained activation energies in the 25 °C to 60 °C temperature range (Table 5). As shown in Table 6, the calculated sample temperatures of the chemical shrinkage tests are slightly higher than the previously estimated values (Table 3). To further demonstrate that the scale factors are indeed associated with the slight temperature differences between chemical shrinkage tests and isothermal calorimetry tests, one of the chemical shrinkage tests (test CS-H-2) was performed by reducing the target temperature (set with the temperature controllers) by 2.8 °C (5 °F). The obtained chemical shrinkage curve of this particular test is found to be directly proportional to the heat evolution curve (i.e., $C = 1$).

At lab temperature (approximately 25 °C), the correlation factor between heat evolution and chemical shrinkage (H^0/CS^0) for the different cements is found to range from 7500 J/mL to 8000 J/mL, well within the previously reported range of 6500–8500 J/mL [33,34]. The correlation factor increases with increasing curing temperature. Since H^0 is independent of curing temperature, the results suggest that CS^0 decreases with increasing temperature, consistent with previous studies [6,10]. In the relatively small temperature range investigated (25–60 °C), the variations of CS^0/H^0 and H^0/CS^0 with temperature can both be approximated by linear models. Fig. 9 shows the dependence of CS^0/H^0 on curing temperature for different types of cement. The least square fits of all data points indicate the average rate of change to be −0.00076 mL/kJ per °C for CS^0/H^0 and +58 J/mL per °C for H^0/CS^0. When normalized to the values at 25 °C, the linear reduction rate of CS^0 with increasing temperature is determined to be 0.57%, 0.65%, 0.58%, 0.66%, and 0.57% per °C for Class A, C, G, H-P, and H-I cements, respectively, suggesting an average reduction rate of 0.60% (with a standard deviation of 0.046%) per °C. For comparison, a reduction rate of 0.78% per °C may be obtained from test data of Zhang et al. [10] in the same temperature range, where the correlations between w_n^0 and CS^0 of Class H cement were investigated.

5. Conclusions

The hydration kinetics of different types of cement cured at different temperatures has been evaluated by both the traditional isothermal calorimetry test method and a newly developed chemical shrinkage test method. A scale factor model that can be used to predict the effect of curing temperature on cement hydration kinetics, previously validated with chemical shrinkage test data, is further discussed and validated with the heat evolution test data. Due to the fact that the different compounds in cement hydrate at different rates and have different temperature sensitivities, the model is found to be more accurate for cement with simpler compositions (e.g., no or very low C_3A content) and/or for smaller temperature changes (e.g. ⩽15 °C). The scale factor model also introduces a new method of estimating the apparent activation energies of Portland cement (i.e. the best-fit method). The apparent activation energies of Classes A, C, G, H-P and H-I cements determined using the heat of hydration data in the temperature range of 25–60 °C are 40.2 kJ/mol, 37 kJ/mol, 40.2 kJ/mol, 35.5 kJ/mol, and 37 kJ/mol, respectively.

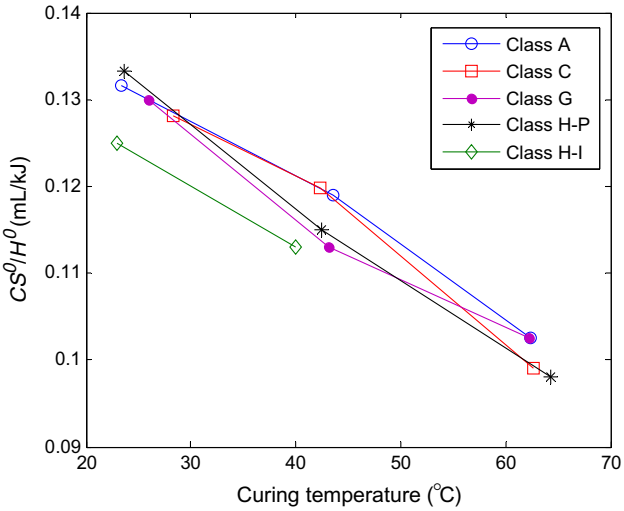

Fig. 9. Dependence of correlation factor (CS^0/H^0) on curing temperature.

A correlation study of chemical shrinkage and isothermal calorimetry test data indicate that total chemical shrinkage is proportional to cumulative heat evolution if the two tests are conducted on the same cement paste at the same curing temperature, in agreement with previous research. The scale factor model discussed in this study can be used to account for any unmeasured small temperature differences. The proportionality constant, namely the ratio of total chemical shrinkage to total heat release at complete hydration (CS^0/H^0), varies slightly with cement composition and decreases with increasing curing temperature. If H^0 is assumed to be independent of curing temperature, then CS^0 decreases approximately linearly with increasing temperature at a rate of 0.600 ± 0.046% per °C from the reference values at 25 °C for the different cements used in this study. Compared to C_3S hydration, early C_3A hydration (typically at the main hydration peak) seems to create a higher ratio of chemical shrinkage to heat evolution, while later C_3A hydration (typically during the deceleration period) appears to create a lower ratio. As a result, the rate of chemical shrinkage curve typically has a slightly different shape than the heat flow curve for cements that contain significant C_3A.

Acknowledgements

The continuous support of this study from Dr. Lewis Norman and Dr. Ron Morgan of Halliburton is cordially appreciated. We thank Mr. David Meadows of Halliburton for his help in developing the chemical shrinkage test apparatus and Ms. Donna Chen of Columbia University for her help in performing part of the experimental work. The critical review of this work by Dr. Jeffrey Bullard of NIST is also greatly acknowledged.

References

[1] Parrott LJ, Geiker M, Gutteridge WA, Killoh D. Monitoring Portland cement hydration: comparison of methods. Cem Concr Res 1990;20:919–26.
[2] Gutteridge WA, Dalziel JA. Filler cement: the effect of the secondary component on the hydration of portland cement: Part I. A fine non-hydraulic filler. Cem Concr Res 1990;20:778–82.
[3] Bentz DP. A three-dimensional cement hydration and microstructure program: I. Hydration rate, heat of hydration, and chemical shrinkage, NISTIR 5756. US Department of Commerce, Washington DC; 1995.
[4] Escalante-Garcia JI. Nonevaporable water from neat OPC and replacement materials in composite cements hydrated at different temperatures. Cem Concr Res 2003;33(11):1883–8.
[5] Lura P, Winnefeld F, Klemm S. Simultaneous measurements of heat of hydration and chemical shrinkage on hardening cement pastes. J Therm Anal Calorim 2010;101(3):925–32.
[6] Geiker M. Studies of Portland cement hydration: measurements of chemical shrinkage and a systematic evaluation of hydration curves by means of the dispersion model. PhD thesis, Technical University of Denmark; 1983.
[7] Mounanga P, Baroghel-Bouny V, Loukili A, Khelidj A. Autogenous deformations of cement pastes: Part I. Temperature effects at early age and micro–macro correlations. Cem Concr Res 2006;36:110–22.
[8] Peethamparan S, Weissinger E, Vocaturo J, Zhang J, Scherer G. Monitoring chemical shrinkage using pressure sensors. Adv Mater Sci Concr ACI SP-270 2010;7:77–88.
[9] Pang X, Meyer C. Cement chemical shrinkage as measure of hydration kinetics and its relationship with nonevaporable water. ACI Mater J 2012;109(3):341–52.
[10] Zhang J, Weissinger EA, Peethamparan S, Scherer GW. Early hydration and setting of oil well cement. Cem Concr Res 2010;40:1023–33.
[11] Scherer GW, Zhang J, Thomas JJ. Nucleation and growth models for hydration of cement. Cem Concr Res 2012;42:982–93.
[12] Pang X, Meyer C, Darbe R, Funkhouser GP. Modeling the effect of curing temperature and pressure on cement hydration kinetics. ACI Mater J 2013;110(2):137–48.
[13] API Specification 10A. Specification for cements and materials for well cementing, American Petroleum Institute; 2010. p. 38.
[14] ASTM C150/C150M – 09. Standard specification for Portland cement. ASTM International, West Conshohocken, PA; 2009. p. 10.
[15] ASTM C1608. Standard test method for chemical shrinkage of hydraulic cement paste. ASTM International, West Conshohocken, PA; 2007. p. 4.
[16] Sant G, Lura P, Weiss J. Measurement of volume change in cementitious materials at early ages: review of testing protocols and interpretation of results. J Trans Res Rec 2006;1979:21–9.
[17] Costoya M. Kinetics and microstructural investigation on the hydration of tricalcium silicate. Doctoral thesis, École Polytechnique Fédérale de Lausanne, Switzerland; 2008.
[18] Pang X. Effects of curing temperature and pressure on the chemical, physical, and mechanical properties of Portland cement. PhD dissertation, Columbia University, New York; 2011.
[19] ASTM C1679. Standard practice for measuring hydration kinetics of hydraulic cementitious mixtures using isothermal calorimetry. West Conshohocken, PA: ASTM International; 2009.
[20] Bentz DP, Ferraris CF. Rheology and setting of high volume fly ash mixtures. Cem Concr Compos 2010;32(4):265–70.
[21] Mills RH. Factors influencing cessation of hydration in water cured cement pastes, special report no. 90. In: Proceedings of the symposium on the structure of Portland cement paste and concrete. Highway Research Board, Washington DC; 1966. p. 406–24.
[22] Mounanga P, Khelidj A, Loukili A, Baroghel-Bouny V. Predicting $Ca(OH)_2$ content and chemical shrinkage of hydrating cement pastes using analytical approach. Cem Concr Res 2004;34:255–65.
[23] Swaddiwudhipong S, Chen D, Zhang MH. Simulation of the exothermic hydration process of Portland cement. Adv Cem Res 2002;14(2):61–9.
[24] Schindler AK, Folliard KJ. Heat of hydration models for cementitious materials. ACI Mater J 2005;102(1):24–33.
[25] Poole JL, Riding KA, Folliard KJ, Juenger MCG, Schindler AK. Methods for calculating activation energy for Portland cement. ACI Mater J 2007;104(1):303–11.
[26] Hewlett PC. Lea's chemistry of cement and concrete. 4th ed. Oxford, England: Butterworth-Heinemann; 1998.
[27] Escalante-Garcia JI, Sharp JH. Effect of temperature on the hydration of the main clinker phases in Portland cements: Part I, neat cements. Cem Concr Res 1998;28(9):1245–57.
[28] Taylor HFW. Cement chemistry. 2nd ed. London, UK: Thomas Telford; 1997.
[29] Bentz DP, Barret T, de la Varga I, Weiss J. Relating compressive strength to heat release in mortars. Adv Civ Eng Mater, in press
[30] ASTM C1074. Standard practice for estimating concrete strength by the maturity method. West Conshohocken, PA: ASTM International; 2010. p. 10.
[31] Bushnell-Watson SM. The effect of temperature upon the setting behaviour of refractory CAC. PhD thesis, University of Sheffield; 1987.
[32] Banfill PFG. Superplasticizers for Ciment Fondu Part 2: effect of temperature on the hydration reaction. Adv Cem Res 1995;7:151–7.
[33] Bentz D, Sant G, Weiss J. Early-age properties of cement-based materials: I. Influence of cement fineness. ASCE J Mater Civ Eng 2008;20(7):502–8.
[34] Bentz DP. Blending different fineness cements to engineer the properties of cement-based materials. Mag Concr Res 2010;62(5):327–38.